Supporting Information

3D-Printed Sodiophilic V_2CT_x/rGO-CNT MXene Microgrid Aerogel for Stable Na Metal Anode with High Areal Capacity

Zixuan Wang,[†] Zhenxin Huang,[†] Hui Wang,[†,‡] Weidong Li,[†] Bingyan Wang,[†] Junmin Xu,[†,*] Tingting Xu,[†] Jinhao Zang,[†] Dezhi Kong,[†] Xinjian Li,[†] Hui Ying Yang,[§,*] Ye Wang[†,*]

[†] Key Laboratory of Material Physics, Ministry of Education, School of Physics and Microelectronics, Zhengzhou University, Zhengzhou 450052, P. R. China

[‡] Center of Super-Diamond and Advanced Films (COSDAF) and Department of Chemistry, City University of Hong Kong, Hong Kong SAR, 999077, P. R. China

[§] Pillar of Engineering Product Development, Singapore University of Technology and Design, 8 Somapah Road, 487372, Singapore

*Corresponding authors: junminxu@zzu.edu.cn (J. Xu); yanghuiying@sutd.edu.sg (H. Y. Yang); wangye@zzu.edu.cn (Y. Wang).

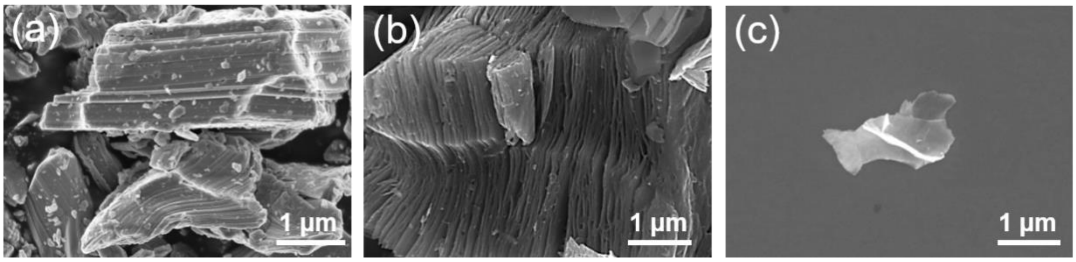

Figure S1. SEM images of (a)V_2AlC MAX phase, (b) multilayer V_2CT_x MXene and (c) a piece of few layers V_2CT_x MXene nanoflake.

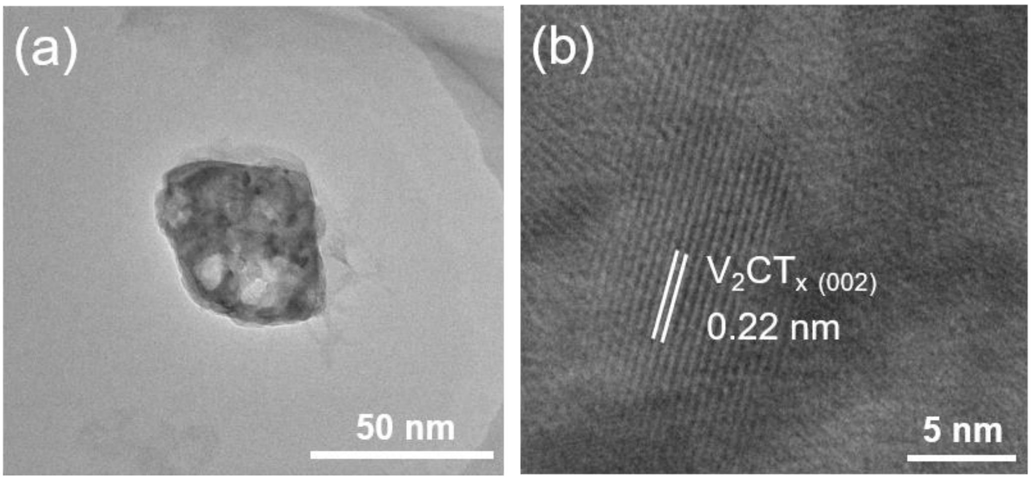

Figure S2. (a) TEM and (b) HRTEM images of V_2CT_x MXene.

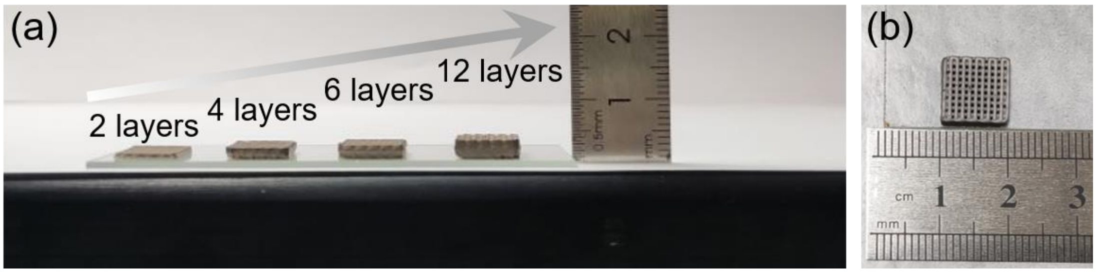

Figure S3. (a) Cross section of multilayers (2-12 layers) and (b) top view of 1 piece of 3D printed V_2CT_x/rGO-CNT microgrid aerogel.

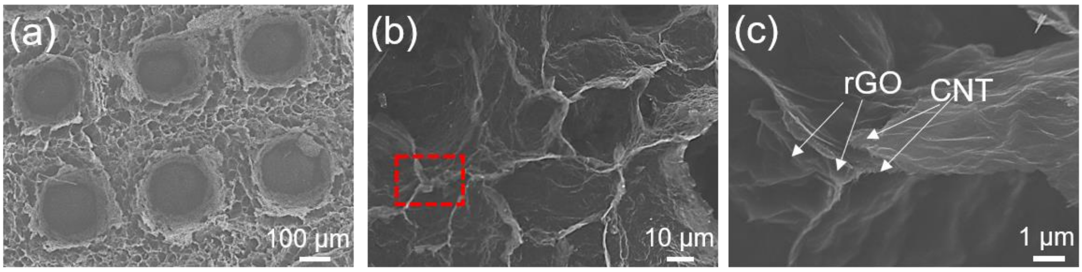

Figure S4. (a-c) SEM images of rGO-CNT microgrid electrode with various magnifications.

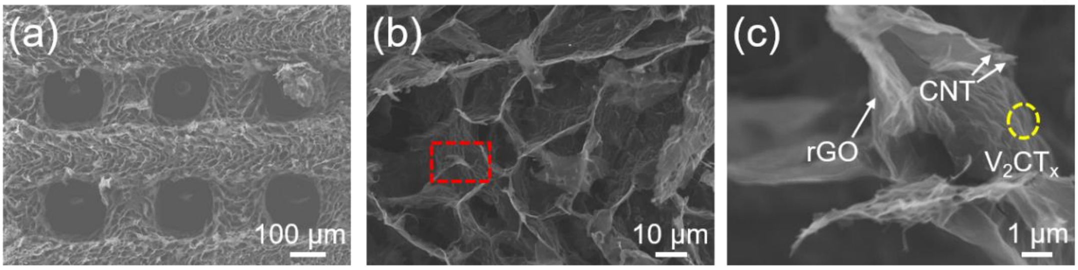

Figure S5. (a-c) SEM images of 10% V_2CT_x/rGO-CNT microgrid electrode with various magnifications.

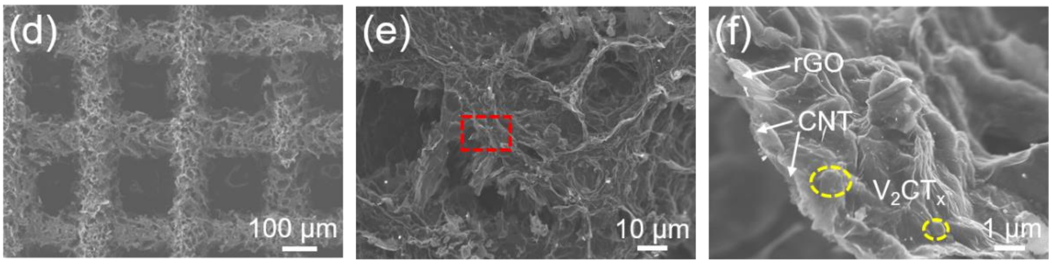

Figure S6. (a-c) SEM images of 50% V_2CT_x/rGO-CNT microgrid electrode with various magnifications.

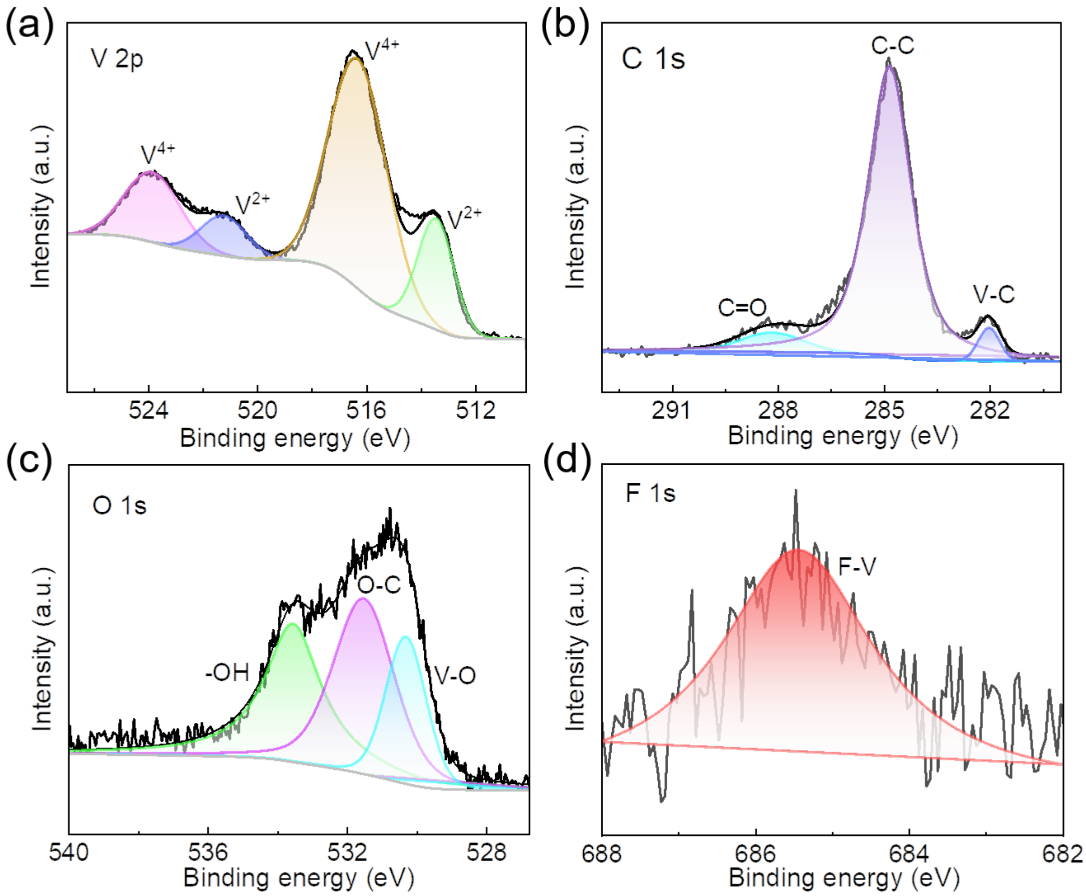

Figure S7. (a) XPS spectra of (a) V 2p, (b) C 1s, (c) O 1s and (d) F 1s of 3D V_2CT_x/rGO-CNT.

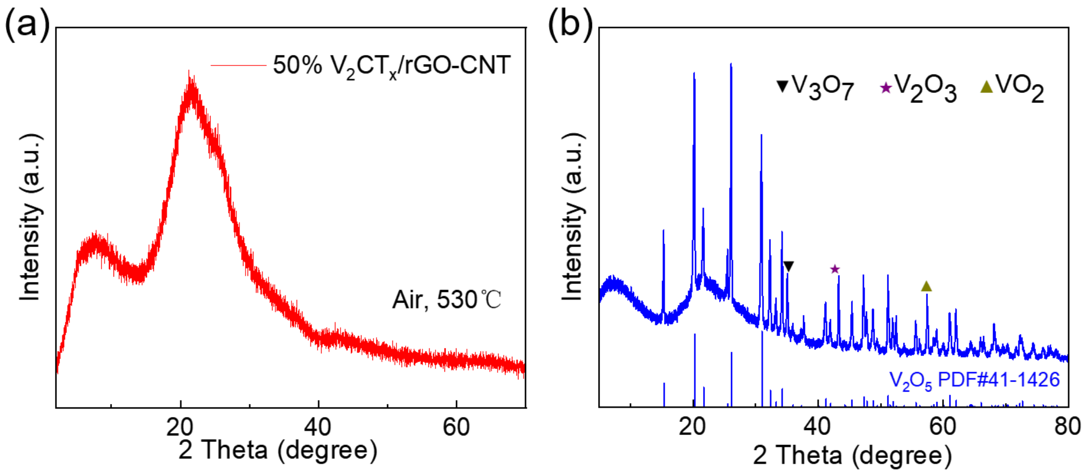

Figure S8. XRD patterns of (a) 50% V_2CT_x/rGO-CNT annealed at 530 ℃ in air and (b) V_2CT_x MXene annealed at 650 ℃ in air.

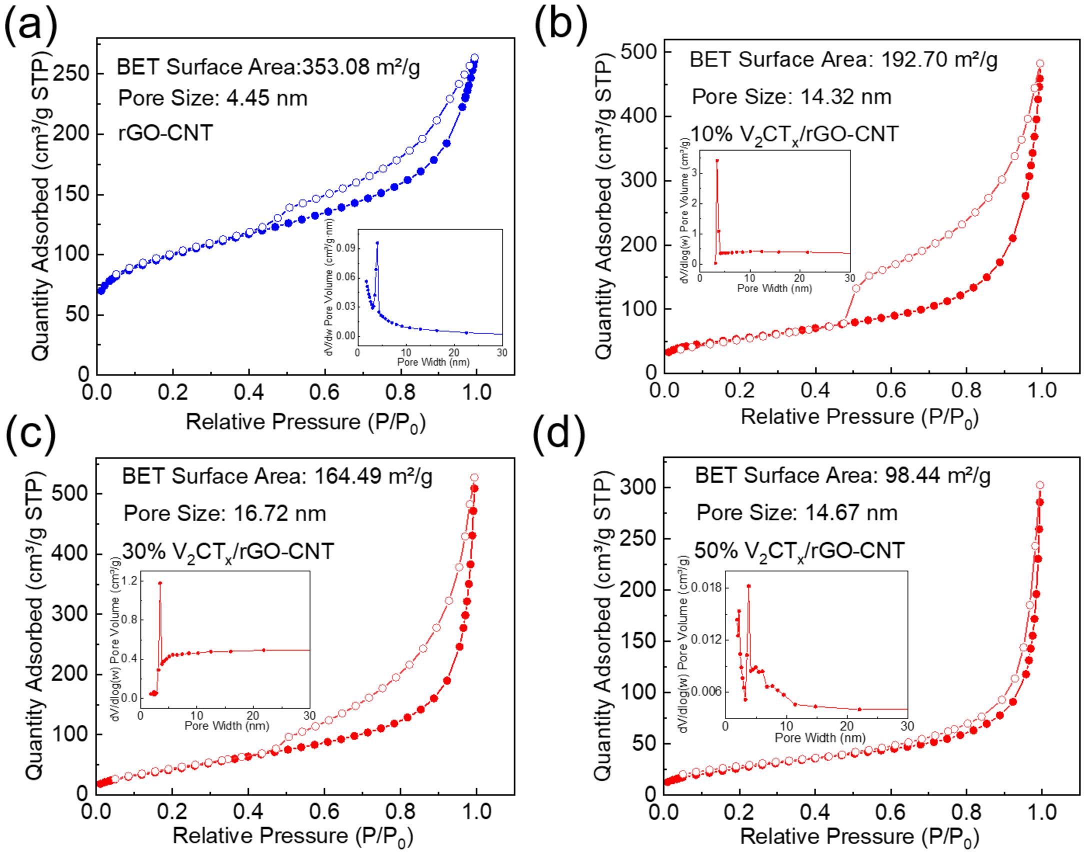

Figure S9. N_2 adsorption/desorption isotherm of 3D printed (a) rGO-CNT, (b) 10% V_2CT_x/rGO-CNT, (c) 30% V_2CT_x/rGO-CNT, (d) 50% V_2CT_x/rGO-CNT microgrid aerogel.

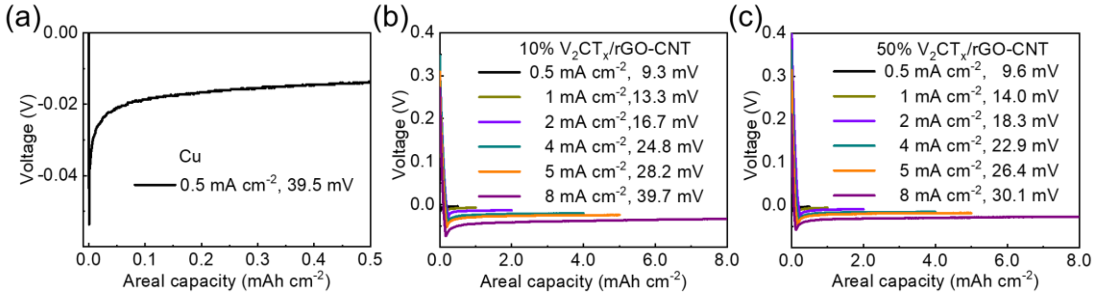

Figure S10. Voltage-capacitance curves of (a) Cu electrode at 0.5 mA cm^{-2}, (b) 10% V_2CT_x/rGO-CNT, (c) 50% V_2CT_x/rGO-CNT microgrid electrodes at different current densities.

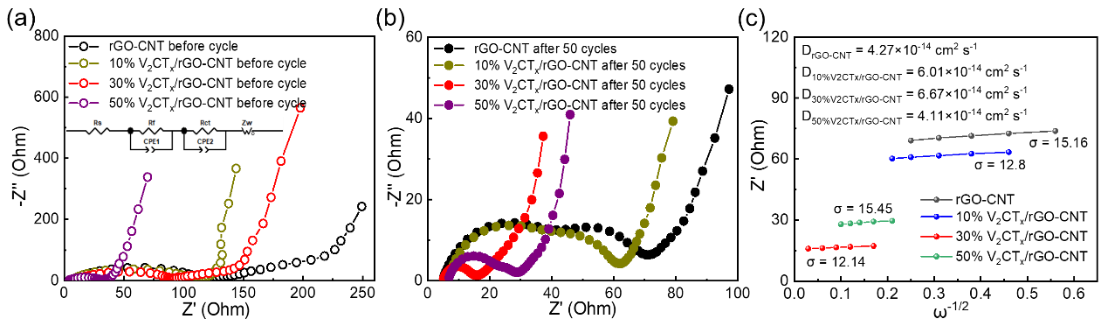

Figure S11. EIS of the rGO-CNT, 10% V_2CT_x/rGO-CNT, 30% V_2CT_x/rGO-CNT, 50% V_2CT_x/rGO-CNT microgrid electrodes (a) before cycle and (b) after 50 cycles. Inset in (a) is the equivalent circuit. R_s, R_f, R_{ct}, CPE and Z_w are the electrolyte resistance, SEI film resistance, charge transfer resistance, constant phase element (CPE) and Warburg impedance. (c) The diffusion coefficients of rGO-CNT, 10% V_2CT_x/rGO-CNT, 30% V_2CT_x/rGO-CNT, and 50% V_2CT_x/rGO-CNT electrodes after 50 cycles calculated based on the EIS data in (b).

The diffusion coefficients of sodium ions on V_2CT_x/rGO-CNT and rGO-CNT electrodes are calculated based on EIS data by the equation:[1-3]

$$D = \frac{R^2T^2}{2A^2n^4F^4C^2\sigma^2}.$$

Where D is the diffusion coefficient, R is the gas constant, T is the absolute temperature, A is the surface area, n is the number of electrons oxidized per molecule, F is the Faraday constant, C is the sodium ion concentration, and σ is the Warburg factor.[1]

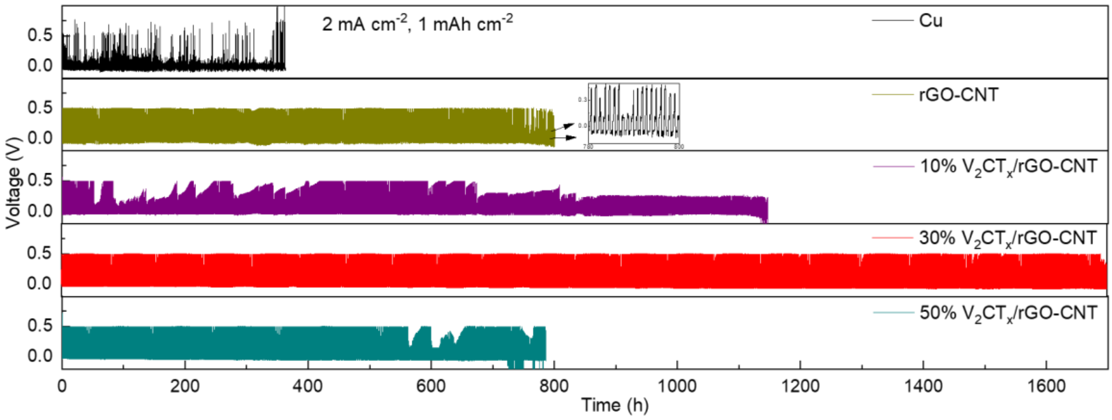

Figure S12. Cycling performance of various electrodes at 2 mA cm^{-2} with 1 mAh cm^{-2}.

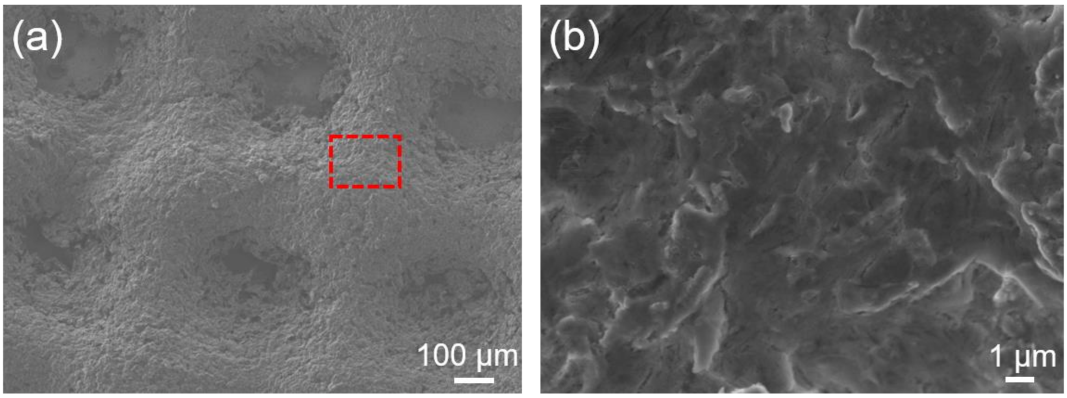

Figure S13. (a, b) SEM images of 3D printed 30% V_2CT_x/rGO-CNT microgrid electrodes after 100 cycles at 2 mA cm^{-2} with 1 mAh cm^{-2} at different magnifications.

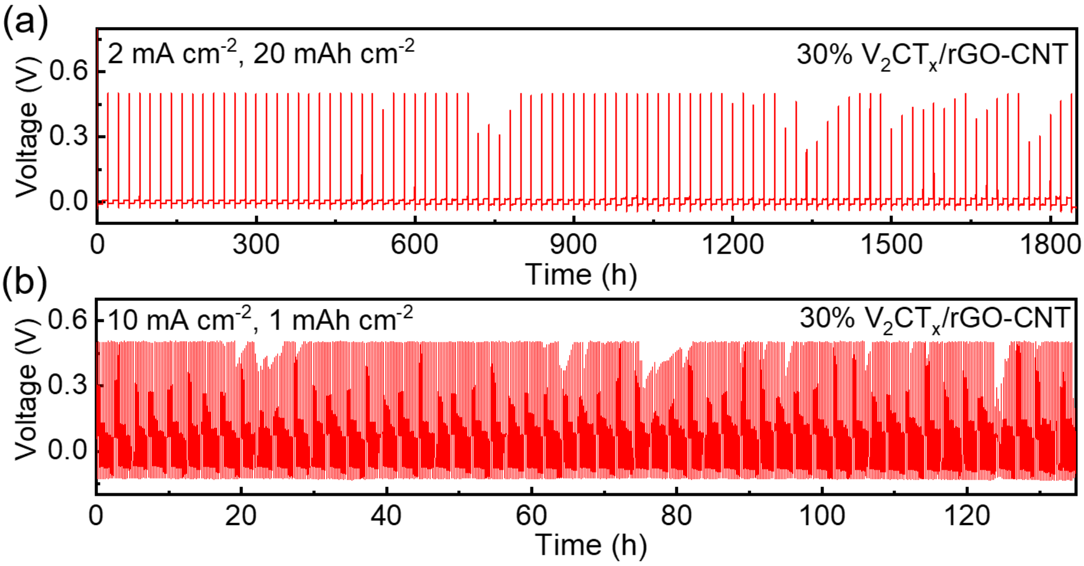

Figure S14. Cycle performance of 30% V_2CT_x/rGO-CNT microgrid electrode at (a) 2 mA cm^{-2} with a high areal capacity of 20 mAh cm^{-2}, and (b) a high current density of 10 mA cm^{-2} with 1 mAh cm^{-2}.

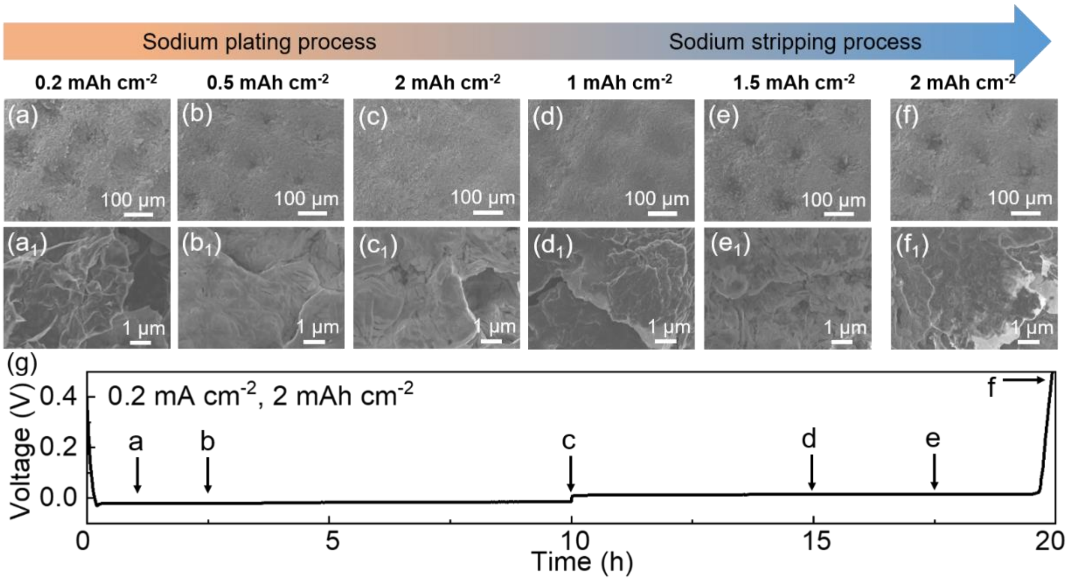

Figure S15. Morphology evolution of Na deposition and stripping on 3D printed rGO-CNT electrodes at 0.2 mA cm^{-2} with the deposition capacities of (a, a_1) 0.2, (b, b_1) 0.5, and (c, c_1) 2 mAh cm^{-2}; with the stripping capacities of (d, d_1) 1, (e, e_1) 1.5, and (f, f_1) 2 mAh cm^{-2}; and (g) corresponding deposition-stripping curve.

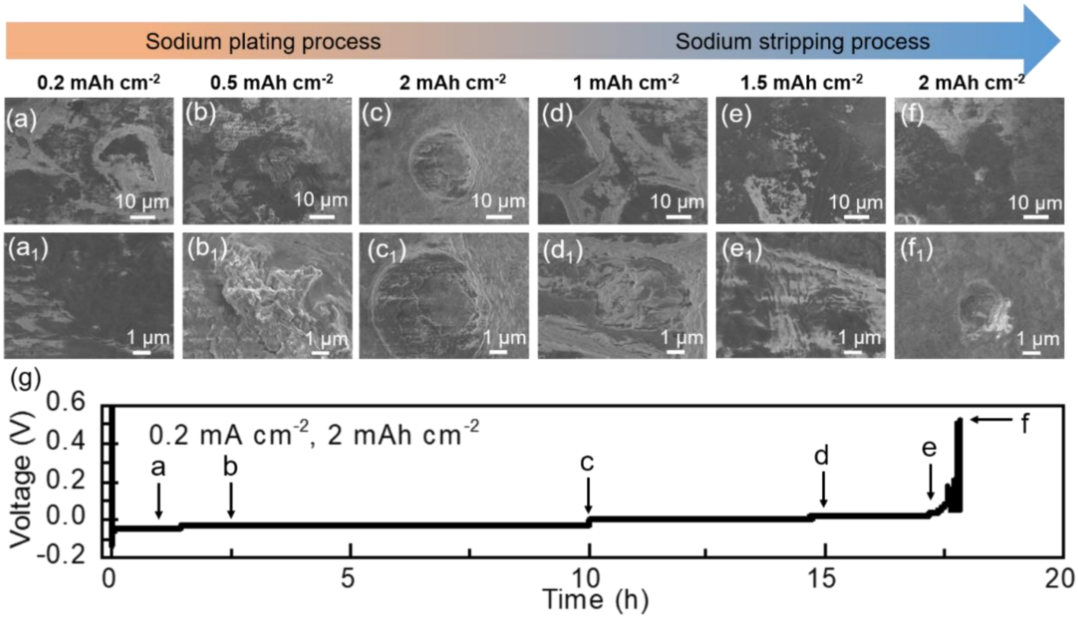

Figure S16. Morphology evolution of Na deposition and stripping on Cu electrode at 0.2 mA cm^{-2} with the deposition capacities of (a, a_1) 0.2, (b, b_1) 0.5, and (c, c_1) 2 mAh cm^{-2}; with the stripping capacities of (d, d_1) 1, (e, e_1) 1.5, and (f, f_1) 2 mAh cm^{-2}; and (g) corresponding deposition-stripping curve.

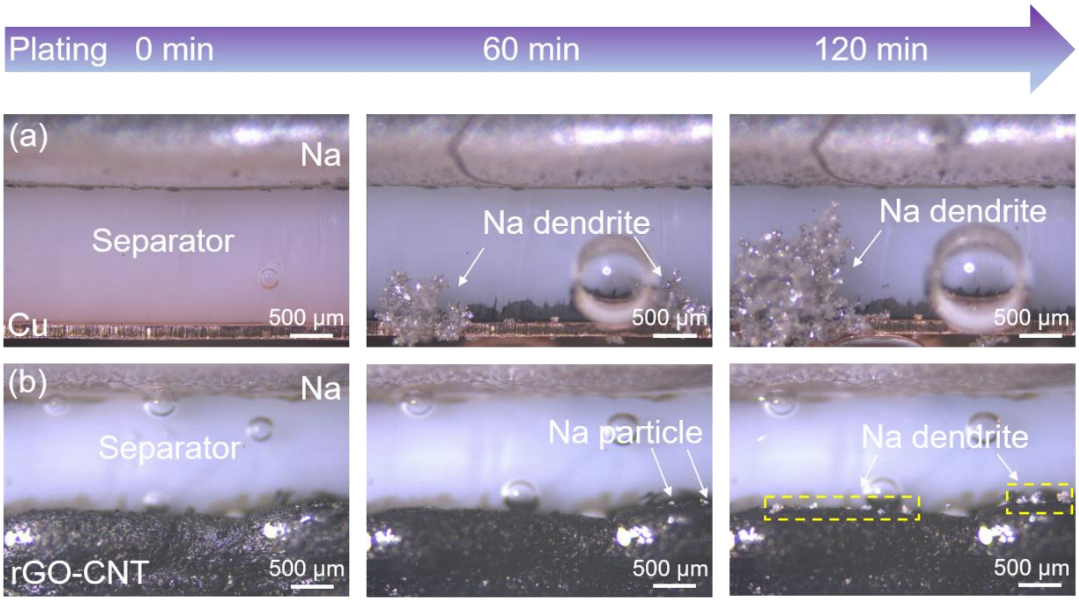

Figure S17. In situ optical images of sodium deposited on (a) Cu foil, (b) rGO-CNT electrodes at 1 mA cm^{-2} for 2 h.

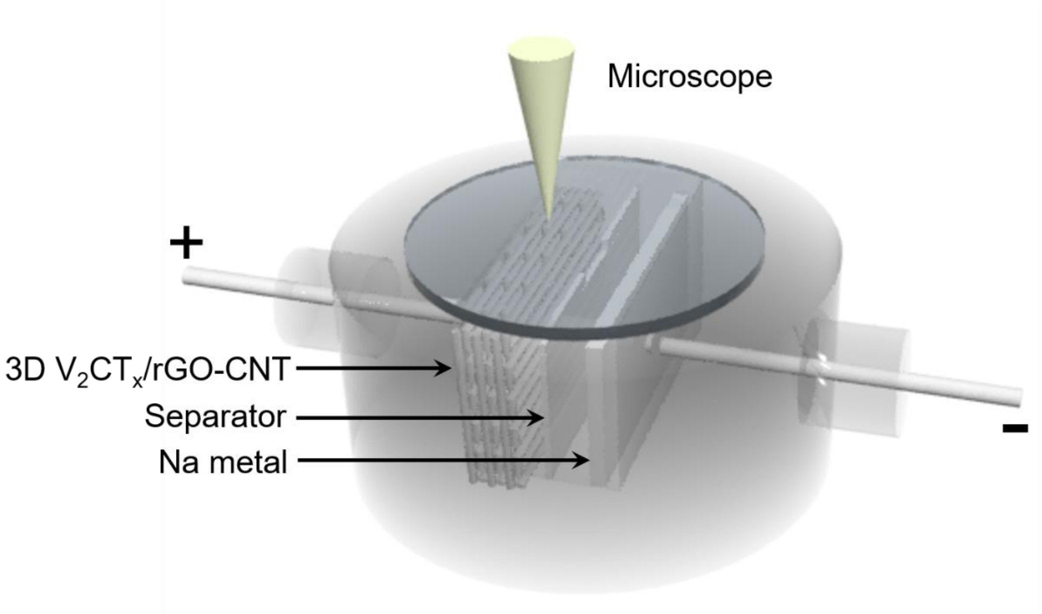

Figure S18. Schematic diagram of in-situ optical microscope testing cell.

Table S1. TGA results to determine the ratio of MXene in various electrodes.

Electrode	Ratios
3D 10% V_2CT_x/rGO-CNT	13.69%
3D 30% V_2CT_x/rGO-CNT	30.38%
3D 50% V_2CT_x/rGO-CNT	46.98%

Table S2. The nucleation overpotentials of various electrodes at the current densities of 0.5-8 mA cm^{-2}. Nucleation overpotential unit: mV.

Current density (mA cm^{-2})	0.5	1	2	4	5	8
3D rGO-CNT	14.6	20.2	25.1	27.6	30.2	40.3
3D 10% V_2CT_x/rGO-CNT	9.3	13.3	16.7	24.8	28.2	39.7
3D 30% V_2CT_x/rGO-CNT	9.6	13.3	16.2	20.1	22.6	29.2
3D 50% V_2CT_x/rGO-CNT	9.6	14.0	18.3	22.9	26.4	30.1

Table S3. Comparison of electrochemical performance of 3D printed graphene based matrices for Na metal anodes.

Electrode	Current density (mA cm^{-2})	Capacity (mAh cm^{-2})	Cycle number	Cycle time (h)	CE (%)	Volumetric capacity density (mAh cm^{-3})	Ref.
3D printed Graphene	1	1	500	1000	99.84	-	4
3D printed rGO/CNT	2 8	1 1	650 640	650 125	-	4 4	5
V_2CT_x/rGO-CNT	**2** **2** **5** **10**	**1** **10** **50** **1**	**1700** **303** **50** **675**	**1700** **3030** **1000** **135**	**99.35** **99.54** **99.96** **99.31**	**6.67** **66.67** **333.33** **6.67**	**This work**

Table S4. Comparison of electrochemical performance of various MXene based Na metal anodes.

Electrode	Current density (mA cm^{-2})	Capacity (mAh cm^{-2})	Cycle number	Cycle time (h)	CE (%)	Volumetric capacity density (mAh cm^{-3})	Ref.
rGO/MXene	1	1	850	1700	-	79.37	6
h-Ti_3C_2/CNTs	1	1	1000	2000	~99.2	52.36	7
	1	1	2000	4000	-	52.36	
	3	3	600	1200	-	157.08	
	5	5	230	460	-	261.78	
	10	1	400	80	-	52.36	
Sn^{2+} pillared MXene	5	5	200	400	98.8	-	8
	10	3	100	60	98.5		
3D MXene-MF	10	10	360	720	-	-	9
$Ti_3C_2T_x$-CC	1	8	56	900	98.5	250	10
	5	1	750	300	-	31.25	
$Ti_3C_2T_x$-rGO	1	1	600	1200	-	21.74	11
	3	1	750	500		21.74	
1D/2D $Na_3Ti_5O_{12}$-MXene	5	20	37	300	-	-	12
	10	5	300	200	98.8		
V_2CT_x/rGO-CNT	**2**	**1**	**1700**	**1700**	**99.35**	**6.67**	**This work**
	2	**10**	**303**	**3030**	**99.54**	**66.67**	
	5	**50**	**50**	**1000**	**99.96**	**333.33**	
	10	**1**	**675**	**135**	**99.31**	**6.67**	

References

(1) Yun, B.-N.; Du, H. L.; Hwang, J.-Y.; Jung, H.-G.; Sun, Y.-K. Improved electrochemical performance of boron-doped carbon-coated lithium titanate as an anode material for sodium-ion batteries. *J. Mater. Chem. A* **2017**, *5*, 2802-2810.
(2) Rudola, A.; Saravanan, K.; Mason, C. W.; Balaya, P. $Na_2Ti_3O_7$: an intercalation based anode for sodium-ion battery applications. *J. Mater. Chem. A* **2013**, *1*, 2653-2662.
(3) Cao, Q.; Zhang, H. P.; Wang, G. J.; Xia, Q.; Wu, Y. P.; Wu, H. Q. A novel carbon-coated $LiCoO_2$ as cathode material for lithium ion battery. *Electrochem. Commun* **2007**, *9*, 1228-1232.
(4) Yu, Y. K.; Wang, Z. Y.; Hou, Z.; Ta, W. R.; Wang, W. H.; Zhao, X. X.; Li, Q.; Zhao, Y. S.; Zhang, Q. Q.; Quan, Z. W. 3D Printing of Hierarchical Graphene Lattice for Advanced Na Metal Anodes. *ACS Appl. Energy Mater.* **2019**, *2*, 3869-3877.
(5) Yan, J.; Zhi, G.; Kong, D.; Wang, H.; Xu, T.; Zang, J.; Shen, W.; Xu, J.; Shi, Y.; Dai, S.; et al. 3D printed rGO/CNT microlattice aerogel for a dendrite-free sodium metal anode. *J. Mater. Chem. A* **2020**, *8*, 19843-19854.
(6) Wang, S.; Liu, Y.; Lu, K.; Cai, W.; Jie, Y.; Huang, F.; Li, X.; Cao, R.; Jiao, S. Engineering rGO/MXene Hybrid Film as an Anode Host for Stable Sodium-Metal Batteries. *Energy Fuels* **2021**, *35*, 4587-4595.
(7) He, X.; Jin, S.; Miao, L.; Cai, Y.; Hou, Y.; Li, H.; Zhang, K.; Yan, Z.; Chen, J. A 3D Hydroxylated MXene/Carbon Nanotubes Composite as a Scaffold for Dendrite-Free Sodium-Metal Electrodes. *Angew. Chem. Int. Ed.* **2020**, *59*, 16705-16711.
(8) Luo, J.; Wang, C.; Wang, H.; Hu, X.; Matios, E.; Lu, X.; Zhang, W.; Tao, X.; Li, W. Pillared MXene with Ultralarge Interlayer Spacing as a Stable Matrix for High Performance Sodium Metal Anodes. *Adv. Funct. Mater.* **2018**, *29*, 1805946.
(9) Shi, H.; Yue, M.; Zhang, C. J.; Dong, Y.; Lu, P.; Zheng, S.; Huang, H.; Chen, J.; Wen, P.; Xu, Z.; et al. 3D Flexible, Conductive, and Recyclable $Ti_3C_2T_x$ MXene-Melamine Foam for High-Areal-Capacity and Long-Lifetime Alkali-Metal Anode. *ACS Nano* **2020**, *14*, 8678-8688.
(10) Fang, Y.; Lian, R.; Li, H.; Zhang, Y.; Gong, Z.; Zhu, K.; Ye, K.; Yan, J.; Wang, G.; Gao, Y.; et al. Induction of Planar Sodium Growth on MXene ($Ti_3C_2T_x$)-Modified Carbon Cloth Hosts for Flexible Sodium Metal Anodes. *ACS Nano* **2020**, *14*, 8744-8753.
(11) Fang, Y.; Zhang, Y.; Zhu, K.; Lian, R.; Gao, Y.; Yin, J.; Ye, K.; Cheng, K.; Yan, J.; Wang, G.; et al. Lithiophilic Three-Dimensional Porous $Ti_3C_2T_x$-rGO Membrane as a Stable Scaffold for Safe Alkali Metal (Li or Na) Anodes. *ACS Nano* **2019**, *13*, 14319-14328.
(12) Luo, J.; Lu, X.; Matios, E.; Wang, C.; Wang, H.; Zhang, Y.; Hu, X.; Li, W. Tunable MXene-Derived 1D/2D Hybrid Nanoarchitectures as a Stable Matrix for Dendrite-Free and Ultrahigh Capacity Sodium Metal Anode. *Nano Lett.* **2020**, *20*, 7700-7708.